Geothermics 44 (2012) 13–22

Contents lists available at SciVerse ScienceDirect

Geothermics

journal homepage: www.elsevier.com/locate/geothermics

Numerical simulation of salt precipitation in the fractures of a CO_2-enhanced geothermal system

Andrea Borgia*, Karsten Pruess, Timothy J. Kneafsey, Curtis M. Oldenburg, Lehua Pan

Lawrence Berkeley National Laboratory (LBNL), 1 Cyclotron Road, MS 90R1116, Berkeley, CA 94720, USA

ARTICLE INFO

Article history:
Received 19 January 2012
Accepted 4 June 2012
Available online 29 June 2012

Keywords:
CO_2-EGS
Geothermal energy
Reservoir modeling
Salt precipitation

ABSTRACT

The development of enhanced geothermal systems using CO_2 (CO_2-EGS) is a promising idea for expanding geothermal energy production (especially in areas with scarce water resources) when large supplies of captured anthropogenic CO_2 may be available in the future. Implementing this concept relies on replacing the natural geothermal brine in the reservoir with injected CO_2 to achieve enhanced energy recovery, and raises the questions of the fate of dissolved salts in the brine as CO_2 dries out the system, and how any precipitated salt could affect fluid flow. In this case, a new TOUGH2 equation of state module (ECO_2H) was used to simulate CO_2 injection in an EGS with a brine system comprised of H_2O and NaCl. This so called CO_2-EGS reservoir is at a depth of 3.5–4.5 km with normal pressure (hydrostatic) and temperature (160–200 °C) gradients. A classic "five-well" geometry is assumed in our 706 m × 706 m × 1 km block, of which only one eighth of the area needs to be modeled due to symmetry. The fractured EGS reservoir was modeled using the multiple interacting continua (MINC) conceptual model with fracture spacing of 10 m. Dry CO_2 was injected at the bottom of the initially brine-saturated reservoir and hot fluids were produced from the top of the reservoir. Simulations show that the brine contained in the fractures is produced initially, and only a few weeks later, the CO_2 plume breaks through at the production well. The two-phase nature of flow at this time causes a reduction in flow rate. Fluid production increases again as the reservoir dries out and the injected CO_2 fills the fractures (and more slowly the matrix). As the produced fluid becomes single-phase CO_2, energy production is enhanced. For salt mass fractions of the order of 0.01 (salinity of 10,000 ppm), total heat produced during the lifetime of the well (about 6 years) is 270% more than that achievable with H_2O as the working fluid. This result is probably at the lower end of what had been previously suggested by Randolph and Saar (2011). Simulation results show that as the brine is driven out of the matrix by capillary pressure, H_2O evaporates into the CO_2 plume and salt precipitates in the fractures clogging up the flow system. At the highest salt mass fraction modeled here (0.15), enhanced energy production is inhibited by halite precipitation in the fractures. Our simulations suggest that for low-salinity systems, significant clogging occurs close to the production well after less than 10 years, while at high salinities clogging occurs close to the injection well in less than one year. Even though clogging of the reservoir is an apparently inevitable consequence of the drying of the saline geothermal reservoir, the fact that clogging occurs in specific reservoir regions could imply that remediation strategies could be developed to mitigate clogging.

Published by Elsevier Ltd.

1. Introduction

It has long been suggested that the use of CO_2 as a working fluid for geothermal heat extraction could be beneficial relative to water (e.g., Brown, 2000; Fouillac et al., 2004) for the following reasons: (1) larger expansivity of CO_2 can generate sufficient buoyancy forces between injection and production wells to drastically reduce power consumption in the fluid circulation system, (2) lower viscosities allow, for any given pressure gradient, larger mass (and heat) extraction rates from the geothermal system, and (3) smaller reactivity with the rocks in the geothermal reservoir, at least in the "dry-CO_2" part of the system.

These technical advantages, along with the convergence of energy-climate priorities, including the need to (a) reduce anthropogenic CO_2 emissions by expanding use of geothermal energy relative to fossil fuels, (b) develop geothermal resources in arid regions where water for injection may be scarce, (c) reduce environmental impact related to excessive drawdown of valuable freshwater aquifers, and (d) utilize or sequester the large amounts of captured anthropogenic CO_2 that may be available in the near

* Corresponding author. Tel.: +1 510 495 2304; fax: +1 510 486 5686.
E-mail address: aborgia@lbl.gov (A. Borgia).

0375-6505/$ – see front matter. Published by Elsevier Ltd.
http://dx.doi.org/10.1016/j.geothermics.2012.06.002

future, have greatly elevated interest in understanding and testing various aspects of using CO_2 in EGS.

The complexities and uncertainties associated with geothermal systems in general, and CO_2-EGS systems in particular, motivate research to understand the key processes of fluid flow and heat extraction. Fractures typically provide the vast majority of the permeability in geothermal systems, which is critical to producing energy. But heat flow to the fractures greatly depends on interactions with the matrix, which makes up the vast majority of the chemical and thermal mass of the system, to provide fluid and heat for energy production. In this study, we numerically model the fracture and matrix interactions when injecting pure CO_2 into a geothermal system with brine-filled fractures. Geochemistry is considered only insofar as NaCl–water dissolution and precipitation reactions are concerned, as these are known to exert a strong control on permeability (Carpita et al., 2006; Giorgis et al., 2007; Kleinitz et al., 2001; Lorentz and Muller, 2003; Xu et al., 2004).

2. Prior work

CO_2-EGS research has been very active in the last several years. Pruess and Azaroual (2006) quantified the thermophysical and dynamic properties that make CO_2 a desirable fluid for geothermal energy extraction. Pruess (2006) presented preliminary modeling of CO_2 injection, production and fractured reservoir development and determined that CO_2 could be up to 50% more efficient than water for geothermal energy exploitation. Atrens et al. (2008, 2009, 2010) attempted to optimize the positive thermosiphon effect that develops in using CO_2 in place of water for geothermal reservoir exploitation. Rosenbauer et al. (2005), Xu et al. (2008, 2010), Xu and Pruess (2010), Wan et al. (2011), and Apps and Pruess (2011) performed one- and two-dimensional thermo-hydrological-chemical (THC) simulations in order to evaluate the feasibility of using CO_2 as a working fluid and stimulation agent for EGS, to assess the dissolution and precipitation reactions which could affect reservoir growth and longevity, and to understand the tradeoffs between power generation and CO_2 sequestration in mineral phases. Magliocco et al. (2011) carried out laboratory experiments to study heat extraction from porous media by means of CO_2. Randolph and Saar (2011) examined a variety of porosity- and fracture-dominated geothermal-reservoir scenarios, and their models suggested using CO_2 as the working fluid could improve thermal energy capture by a factor of 2.9–5. Pritchett (2009), however, performed numerical simulation studies to evaluate and compare heat extraction from H_2O- and CO_2-based EGS, finding larger heat recovery for water-based systems, because CO_2 will exacerbate "short-circuiting", that is flow circulation in only a limited volume of the geothermal reservoir.

3. Conceptual and dimensional models

In our conceptual model, dry CO_2 was injected into a water-saturated geothermal reservoir to produce hot fluids for geothermal energy exploitation. Because the development of the CO_2 reservoir causes the system to evolve from being water dominated to supercritical-CO_2 dominated, salt saturation in the water, and consequent precipitation and permeability reduction, are among the major processes that may affect the effective fluid volume and longevity of the reservoir.

The simulation domain consists of a 1 km-thick homogeneous volume of low-permeability rock (comparable to that of a granite), whose permeability is artificially enhanced by dissolution, fracturing and/or fracture reactivation. Such a thick reservoir is chosen to take maximum advantage of the hot-CO_2-plume buoyancy in order to increase fluid and heat production. The rock has a (conductive) geothermal gradient of 40 °C/km (somewhat larger than normal) from a surface temperature of 20 °C and hydrostatic pressure with the top of the system at a depth of 3.5 km. This choice of depth is arbitrary and reflects depth, and temperature and pressure gradients of potential EGS locations. We use the common five-well geometric arrangement extended on the horizontal plane to "infinity" for production and injection (Pruess, 2006; Fig. 1). Because of the symmetry of this arrangement and the assumption of an impermeable cap rock at top and bottom, the triangular parallelepiped model domain (1/8 of a cube) has no-flow boundaries on all sides. These simplifications allow focus on salt precipitation effects and their influence on heat production rather than on the effects of geometry. The actual model size is 0.5 km in the horizontal direction between the injection and production wells and 0.25 km perpendicular to this direction (Fig. 2). Therefore, the total reservoir volume is eight times the actual volume modeled (0.5 km^3).

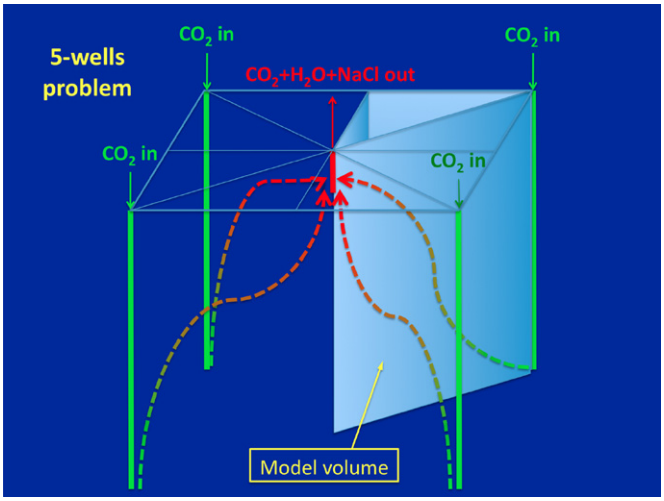

Fig. 1. Five-well geometry of the model volume. Because of the intrinsic symmetry of our system only one-eighth of the total volume is used for the model. Dashed green-to-red thick lines are an idealized description of the CO_2 flow from cold at injection to hot at production. (For interpretation of the references to color in this figure legend, the reader is referred to the web version of this article.)

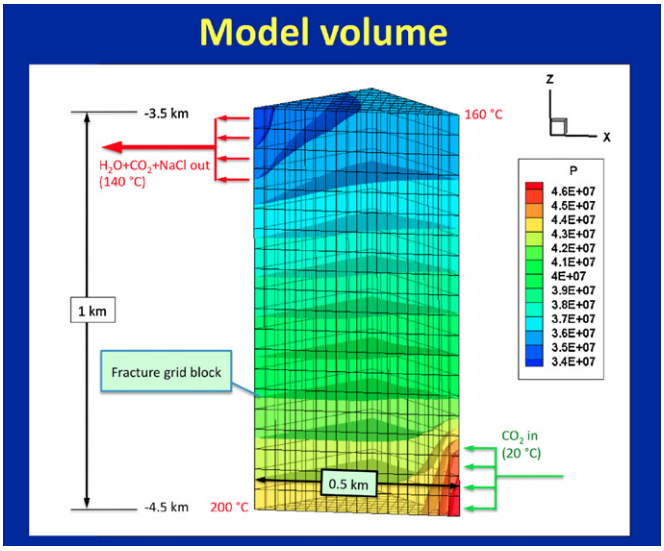

Fig. 2. Geometry, initial and boundary conditions of the model volume. The 3D plot of pressure distribution after 0.2 years shows the production (upper left) and injection (lower right) pressures which are 2 MPa below and above hydrostatic pressure, respectively.

Table 1
Primary variables, initial conditions, and well boundary conditions.

	Pressure, P (MPa)	Salt mass fraction, X_{sm}	Gas ($scCO_2$) saturation, S_g	Temperature, T (°C)
Reservoir min.	35	0.01	0.00	160
Reservoir max.	Hydrostatic	0.15	0.00	200
Injection well	2 above hydrostatic	0.00	1.00	20
Production well	2 below hydrostatic	Produced fluid	Produced fluid	Produced fluid

Table 2
Multiple interacting continua (MINC) parameters (see Appendix A).

Continuum shell	Shell thickness (m)	Shell volume (m^3)	Total volume in grid block (m^3)	Volume fraction
Fracture	0.0010	6.0000E+00	1.8750E+02	0.0060
Matrix 1	0.1137	6.6266E+01	2.0708E+03	0.0663
Matrix 2	0.2447	1.3253E+02	4.1417E+03	0.1325
Matrix 3	0.5867	2.6507E+02	8.2833E+03	0.2651
Matrix 4	1.6218	5.3014E+02	1.6567E+04	0.5301
Total	2.57	1.0000E+03	3.1250E+04	1.0000
Fracture spacing	10.0000			

Results of energy extraction are given for the total reservoir volume. Initial conditions of the system are given in Table 1.

In order to simulate flow in fractures and in the matrix pores, a dual-porosity (Warren and Root, 1963) multiple interacting continua (MINC; Pruess and Narasimhan, 1982, 1985) model (Table 2) was used. Both matrix pores and fractures are assumed to be initially brine saturated with no CO_2. The NaCl mass fraction (X_{sm}) in water was varied from 0.01, corresponding to 10,000 ppm TDS [the salinity limit for protection as a groundwater resource under the Safe Drinking Water Act (U.S. EPA, 1974)], to 0.15, corresponding to a salinity not remarkably high for geothermal reservoirs, but sufficient for illustrating the effects of drying a high-salinity aquifer. Because the CO_2 supercritical phase is very buoyant in water, we injected CO_2 in the bottom part at the right-hand side, and produced fluid (H_2O and CO_2) with dissolved NaCl in proportions which vary with time, from the upper left-hand side of the domain (Fig. 2). We used functions for relative permeability of two-phase flow, employed capillary pressure as shown in Table 3 [see Pruess et al. (1999)]. In addition, we considered halite precipitation and consequent permeability reduction in both fractures and matrix by the methods described in Verma and Pruess (1988).

4. Thermophysical model

The TOUGH2 equation of state module ECO_2H used for our simulations is an extension of the ECO_2N module (Pruess and Spycher, 2007, 2010) taken to higher temperatures appropriate for geothermal systems. ECO_2H includes a comprehensive description of the thermodynamic and thermophysical properties of the H_2O–NaCl–CO_2 system that reproduces fluid properties largely within experimental errors for temperature and pressure, in the range of $10 \leq T \leq 243$ °C and $P \leq 67.6$ MPa respectively, and salinity from zero up to full halite saturation. In particular, ECO_2H can describe a variety of phase conditions for brine–CO_2 mixtures, including transitions between super- and sub-critical conditions. It does not model the phase change between liquid and gaseous CO_2. Flow processes can be non-isothermal, and phase conditions represented may include a single (aqueous or CO_2-rich) phase, as well as two and three-phase mixtures of an aqueous phase, a liquid-like gas-like or supercritical CO_2-rich phase, and a halite solid phase. Solid, aqueous and CO_2-rich phases may appear or disappear in the course of a simulation, and solid salt may precipitate or dissolve.

In the specific model system considered here, given the pressure is everywhere higher than the critical pressure for CO_2, the possible phases present are halite, an aqueous brine, and a liquid-like or supercritical CO_2-rich phase. Under no circumstances can a liquid/gas phase transition occur in the model. At the injection well, the CO_2 is in a liquid state, but it becomes supercritical as it warms during flow through the geothermal reservoir toward the production well.

To compare the heat produced by CO_2-EGS with that produced by an equivalent brine saturated system, a similar system was modeled injecting only a brine with the same salinity as the one extracted (no CO_2 injection). For the range of salinities investigated, the reinjection of brine produces no salt precipitation.

5. Numerical model

The model reservoir volume is subdivided into grid-blocks 25 m × 25 m in the horizontal directions and 50 m high. Therefore, on any of the 20 horizontal triangular layers, there are 110 grid blocks, for a total of 2200 grid blocks. The dual-porosity MINC approach used in the simulations is described in Appendix A. Specific geometric parameters of fracture and matrix MINC grid sub-blocks are given in Table 2. With this subdivision scheme, the model has a total of 11,000 grid-sub-blocks.

Table 3
Parameters used for two-phase permeability reduction (Corey, 1954), capillary pressure (van Genuchten, 1980), and permeability reduction due to salt precipitation (Verma and Pruess, 1988).

Corey's function		Van Genuchten's function		Verma and Pruess's function	
Parameter	Value	Parameter	Value	Parameter	Value
Relative liquid saturation, S_{lr} (fraction)	0.30	l	0.40	g	0.80
Relative gas saturation, S_{gr} (fraction)	0.05	$S_{lrvg} < S_{lr}$ (fraction)	0.00	G	0.80
		$1/P_0$ (fractures) (1/Pa)	2.50E−04		
		$1/P_0$ (matrix) (1/Pa)	1.50E−06		
		Maximum capillary pressure, P_{max} (Pa)	−1.00E−08		
		S_{ls}	1.00		

Table 4
Rock properties of modeled reservoir. Matrix sub-blocks permeability is taken as that of a granite. Fracture block permeability is averaged over the block volume (Pruess, 2006).

Rock continuum	Density (kg/m^3)	Porosity	Permeability (m^2)	Rock heat conductivity (W/(m °C))	Rock grain specific heat (J/(kg °C))
Fractures	2650	0.5	5.00E−14	2.1	1000
Matrix	2650	0.01	2.00E−18	2.1	1000

The injection and production wells are simulated as the first matrix MINC grid sub-block with time-independent Dirichlet (constant-property) boundary conditions. In these grid blocks, no conservation equations are set up, and the primary thermodynamic variables remain unchanged throughout the simulation. Using this approach, one can also simulate around the wells a larger fracture-permeability relative to that of the actual reservoir to avoid pinch-point effects. Thermo-physical conditions are kept constant in the production and injection wells (Atrens et al., 2010; Pruess, 2006).

The primary thermodynamic variables at the injection and production wells are given in Table 1 and the rock properties used are given in Table 4. Worth noting is that wellbore salt mass fraction, CO_2 phase saturation fraction, and temperature are less than or equal to those found in the model reservoir, allowing the flow of mass and energy from the reservoir into the production well (inhibiting flow in the opposite direction).

In addition, the following steps and assumptions were used in our simulations (cf. Pruess et al., 1999; Table 3):

(1) relative permeability of the two phases (gaseous and aqueous) are calculated according to the Corey function (Corey, 1954);
(2) capillary pressure is found according to the van Genuchten function (van Genuchten, 1980);
(3) permeability reduction due to salt precipitation is modeled using the Verma and Pruess (1988) function with complete pore clogging occurring at salt saturation at 20% of the pore space of both matrix and fracture continua;
(4) Klinkenberg diffusivity enhancement is not considered since, at the supercritical pressures of the simulation models, this effect has at most a magnitude in the order of a few percent (Pruess et al., 1999);
(5) dry CO_2 at constant pressure of 2 MPa above hydrostatic and temperature of 20 °C, is injected;

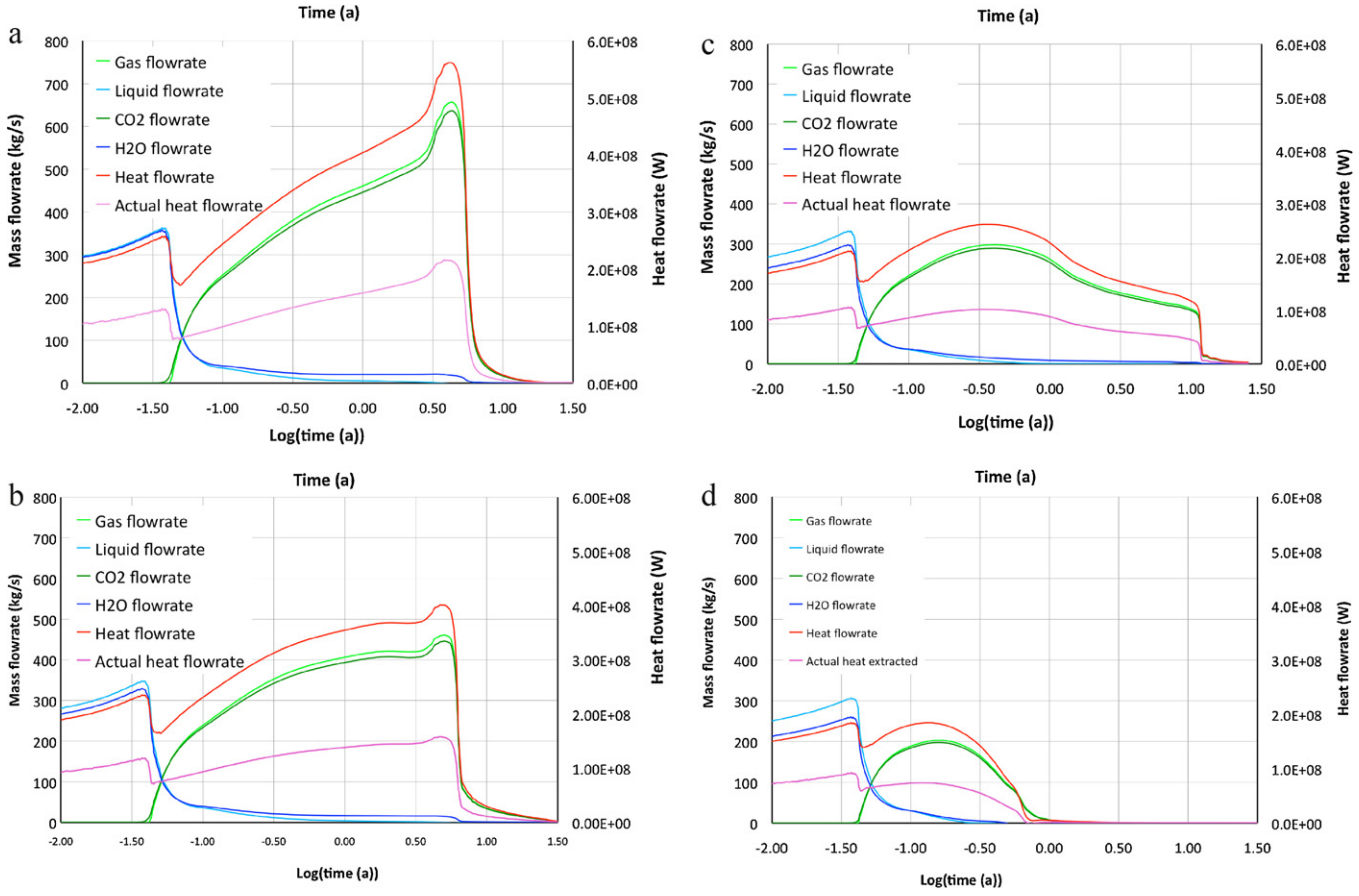

Fig. 3. Flow rates calculated for the full five-well domain at the central production well (see Fig. 2 and Table 5 for variable definitions) for various salt mass fractions (X_{sm}): (a) X_{sm} = 0.01, (b) X_{sm} = 0.05, (c) X_{sm} = 0.10 and (d) X_{sm} = 0.15. Note in all of them, there are two time intervals where production drops; the first due to two-phase flow, the second due to reservoir clogging. Note, also, how the flow rates decrease substantially with the increase in salinity. Instead, while the "life" of the reservoir increases slightly with salinity for the lower 3 salinities, for the highest salinity the reservoir "dies" after less than 1 year. This is due to clogging, which occurs close to the production well for the lower salinities and close to the injection well for the higher salinities. Finally, we observe how there is salt in the liquid at the beginning and H_2O in the gas towards the end of production.

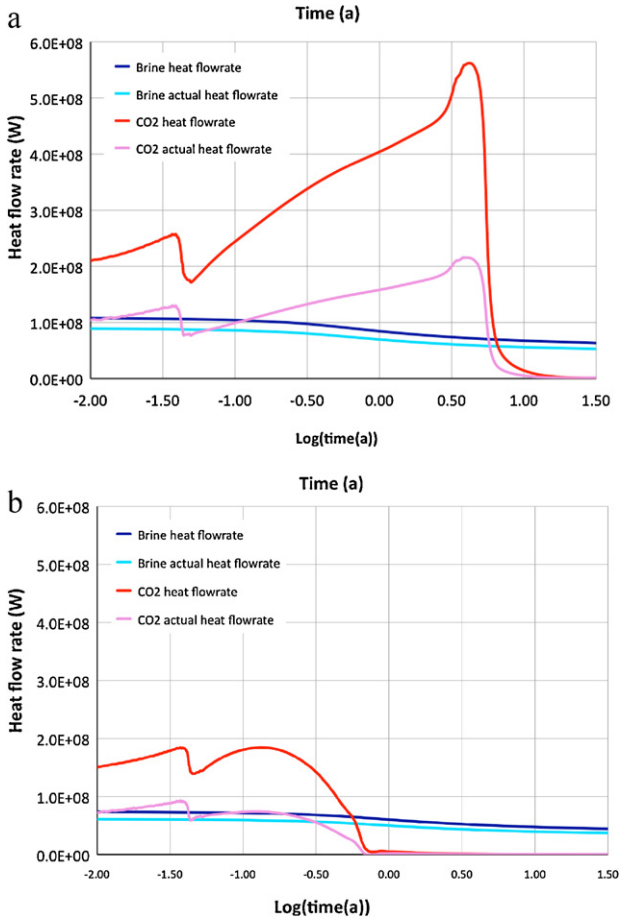

Fig. 4. Heat flow rates and actual heat extracted calculated for the full five-well problem at the central production well (see Fig. 2 and Table 5 for variable definitions) for minimum and maximum salt mass fractions (X_{sm}): (a) $X_{sm} = 0.01$ and (b) $X_{sm} = 0.15$. In addition to CO_2-EGS heat production, we show the curves for heat production by re-circulating the brine extracted from the reservoir (dark and light blue curves). Note that in this second case, the decrease in efficiency due to higher salinities is relatively small compared to the decrease that occurs for CO_2-EGS. (For interpretation of the references to color in this figure legend, the reader is referred to the web version of this article.)

(6) hot fluid at a pressure of 2 MPa below hydrostatic is produced at a constant rate (see Fig. 2).

6. Model results

The model results are shown with two sets of figures: the first set (Figs. 3 and 4) describes the time evolution of variables at the production well, while the second set (Figs. 5–7) describes the 3D distribution of variables at $t = 0.2$, 1, 5, and 25 years.

In Fig. 3 we show the variations in time of aqueous phase and H_2O-component flow rates, of supercritical CO_2-rich and CO_2 component flow rates, and of heat produced and actual heat extracted (see Table 5 for definitions). The figure shows that for all salinities, one can identify the following five time periods:

(1) The first period is characterized by an increase in produced liquid and heat flow rate, with the liquid composed of H_2O + NaCl. The increase in flow rate results from the displacement of the aqueous brine contained in the rock by CO_2. In fact, because CO_2 is less viscous than water, it flows more easily through the fractures, thereby propagating pressure farther into the reservoir, and effectively producing a larger pressure gradient near the production well where the more-viscous brine is being produced.

(2) After a few weeks, the CO_2 plume reaches the production well inducing two-phase flow in the fractures around the well, and a concomitant decrease in effective permeability for both aqueous and supercritical phases. This effect forces a reduction of about 25% in mass and heat flow rates at the production well for all salinities. We observe that the heat flow rate reduction is not as drastic as the one suggested by Pruess and Spycher (2010), and Wan et al. (2011) for two-dimensional planar systems. We believe this to be the result of including buoyancy forces in our model and a multi-layer production 600 m above injection. We also note that the CO_2 component reaches the production well before the CO_2 plume, because it dissolves and diffuses into the water ahead of the plume itself.

(3) After the first decrease in heat production, because the brine dries out in the fractures close to the production well, the effect of two-phase flow decreases and the CO_2 mass flow rate starts to grow again increasing the production of heat.

(4) When the liquid water completely dries out (roughly after 3 years), there is an additional increase in heat production. This is because there is no more permeability reduction due to two-phase-flow in most of the reservoir, and the well-known advantageous properties of CO_2 as a heat transfer fluid take over.

(5) Right after drying (at around 5 years from start in the lower salinity cases), halite begins to precipitate in the fractures, significantly clogging the system and inhibiting CO_2 flow. As a consequence, the produced heat drops by at least an order of magnitude.

Comparing the results for various salinities show that as the salinity increases, there is a general drop in flow rates, particularly during period 4 (Fig. 3). The time at which clogging occurs, though, becomes larger with increasing salinity because salt precipitation will tend to occur throughout the reservoir before clogging occurs at the production well. Only at the highest salinity (Fig. 3d) salt precipitation becomes drastic, even at times smaller than 1 year, clogging the reservoir around the injection well.

Comparing the actual heat produced when using CO_2 and the extracted brine as the working fluid (Fig. 4) shows that the decrease in productivity as a function of salt concentration in the brine is substantially more pronounced for the CO_2 case relative to the brine case. In other words, the decrease in efficiency due to higher salinities is relatively small, if the geothermal aquifer brine is used as the working fluid, and it is much larger for CO_2-EGS because of salt precipitation. This effect reduces the efficiency of CO_2-EGS, at the highest salinities modeled here, to values smaller than those obtained from H_2O-EGS for an equal period of well productivity.

The second set of figures shows the 3D and time distribution of CO_2 phase saturation (Fig. 5), NaCl mass fraction in liquid (Fig. 6), and solid (halite) saturation (Fig. 7 and Table 5), both in the fracture and first matrix shells at the two extreme salt mass fractions in the liquid ($X_{sm} = 0.01$ and $X_{sm} = 0.15$). The CO_2-rich (supercritical) saturation plots that show the evolution of the CO_2 plume in the reservoir are used to make the following observations:

(a) At low salinity (Fig. 5a), the plume grows relatively fast from the injection well towards the top of the reservoir and the production well. After just 0.2 years, there is two-phase flow in most of the reservoir, while close to the injection well the CO_2 plume has already dried out the reservoir. After 1 year, at least one-third of the reservoir has been dried out. Comparing the gas saturation in fractures with that in the matrix at either time

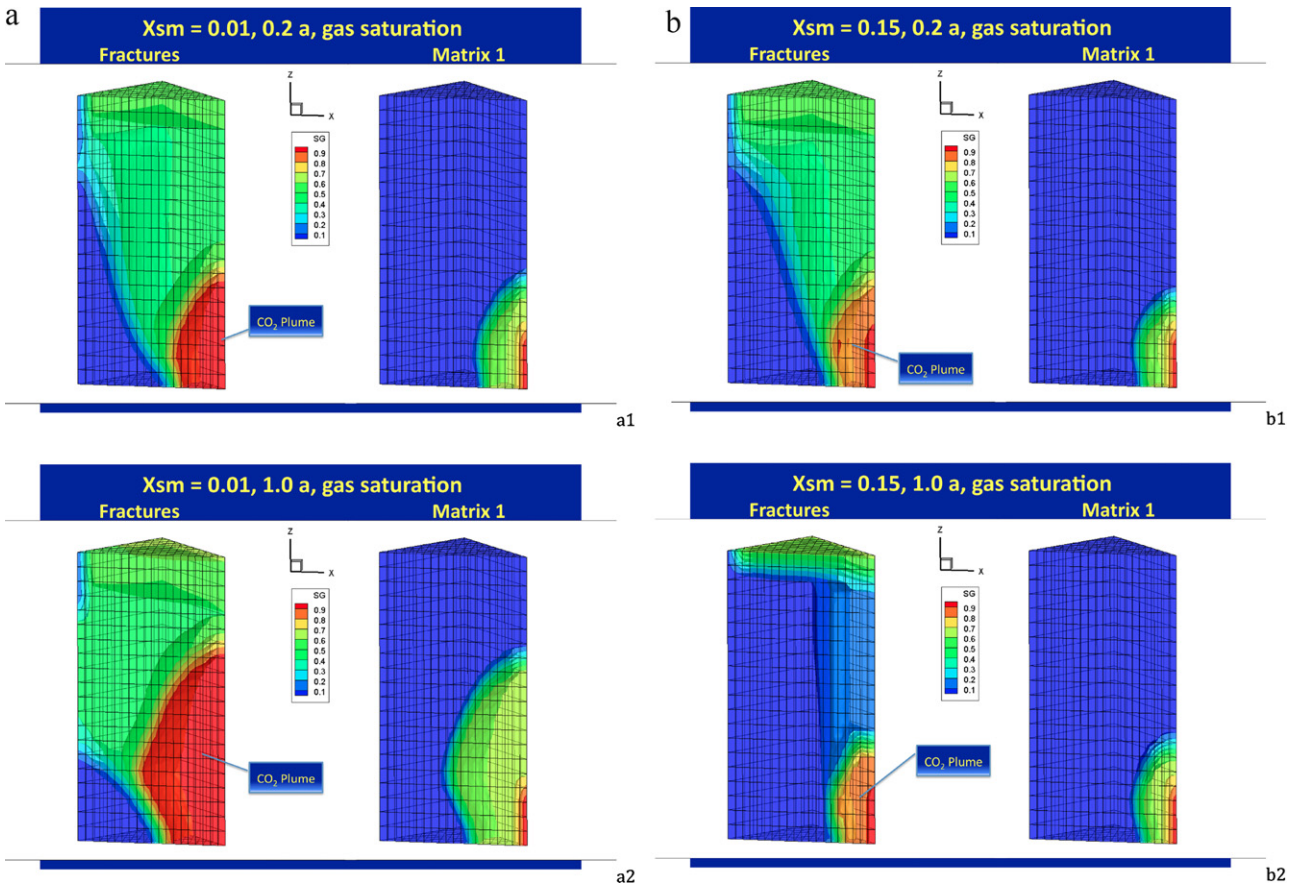

Fig. 5. Gas saturation in the fracture and 1st matrix continua after 0.2 and 1 year, for a salt mass fraction of (a) 0.01 and (b) 0.15 (see Table 5 for variable definitions). The CO_2 plume has already reached the production well. (a) Note how in the matrix the plume grows much more slowly than in the fractures. (b) Note how the CO_2 plume remains "trapped" close to the injection well.

shows that the gas is penetrating into the matrix and displacing water very slowly.

(b) At high salinity (Fig. 5b), the CO_2 plume grows more slowly than at low salinity, and after 1 year it has practically become immobile, remaining confined in the proximity of the injection well.

The plots of the salt mass fraction in the liquid (Fig. 6) show the time evolution of NaCl concentrations. It is observed that:

(a) At low salinity (Fig. 6a), salts become concentrated in a "shell" that envelopes the dry CO_2 plume. This salty envelope has concentrations of about $X_{sm} = 0.2$ and moves ahead of the plume until it reaches the production well in less than 5 years.

(b) At high salinity (Fig. 6b), salt becomes concentrated in the water throughout the reservoir reaching values of $X_{sm} = 0.2$ from the original value of $X_{sm} = 0.15$. A salty envelope develops in front of the CO_2 plume in this case as well, with concentrations reaching close to $X_{sm} = 0.26$. After one year, a large, low-salinity zone forms close to the production well because of water condensing out of the fading CO_2 plume and thereby diluting the saline water in the liquid (aqueous) phase.

The solid saturation within the matrix and the fractures of the reservoir rock shows the clogging effect produced by the precipitation of halite in the fractures:

(a) At low salinity (Fig. 7a), salt begins to precipitate in the fractures right behind the CO_2 plume front, while almost no salt

Table 5
Definition of variables used in the model.

Variable	Symbol	Units	Definition
Pressure	P	Pa	Pressure of the fluid in the rock pores
Temperature	T	°C	Temperature of rock and fluid
Gas flow rate	Q_g	kg/s	Flow rate of supercritical and liquid-like H_2O-rich CO_2
Liquid flow rate	Q_l	kg/s	Flow rate of CO_2-rich brine
CO_2 flow rate	Q_{CO_2}	kg/s	Flow rate of CO_2 component in both gas and liquid phases
H_2O flow rate	Q_{H_2O}	kg/s	Flow rate of H_2O component in both liquid and gas phases
Heat flow rate	Q_h	W	Total heat flow rate at production or injection wells
Actual heat flow rate	ΔQ_h	W	Heat flow rate at production minus injection wells
Gas saturation	S_g		Volumetric fraction of gas in matrix and fracture pores
Solid saturation	S_s		Volumetric fraction of halite in the pores of the matrix or in the fracture continua
NaCl mass fraction	X_{sm}, X_{NaCl}		Mass fraction of salt in the liquid phase

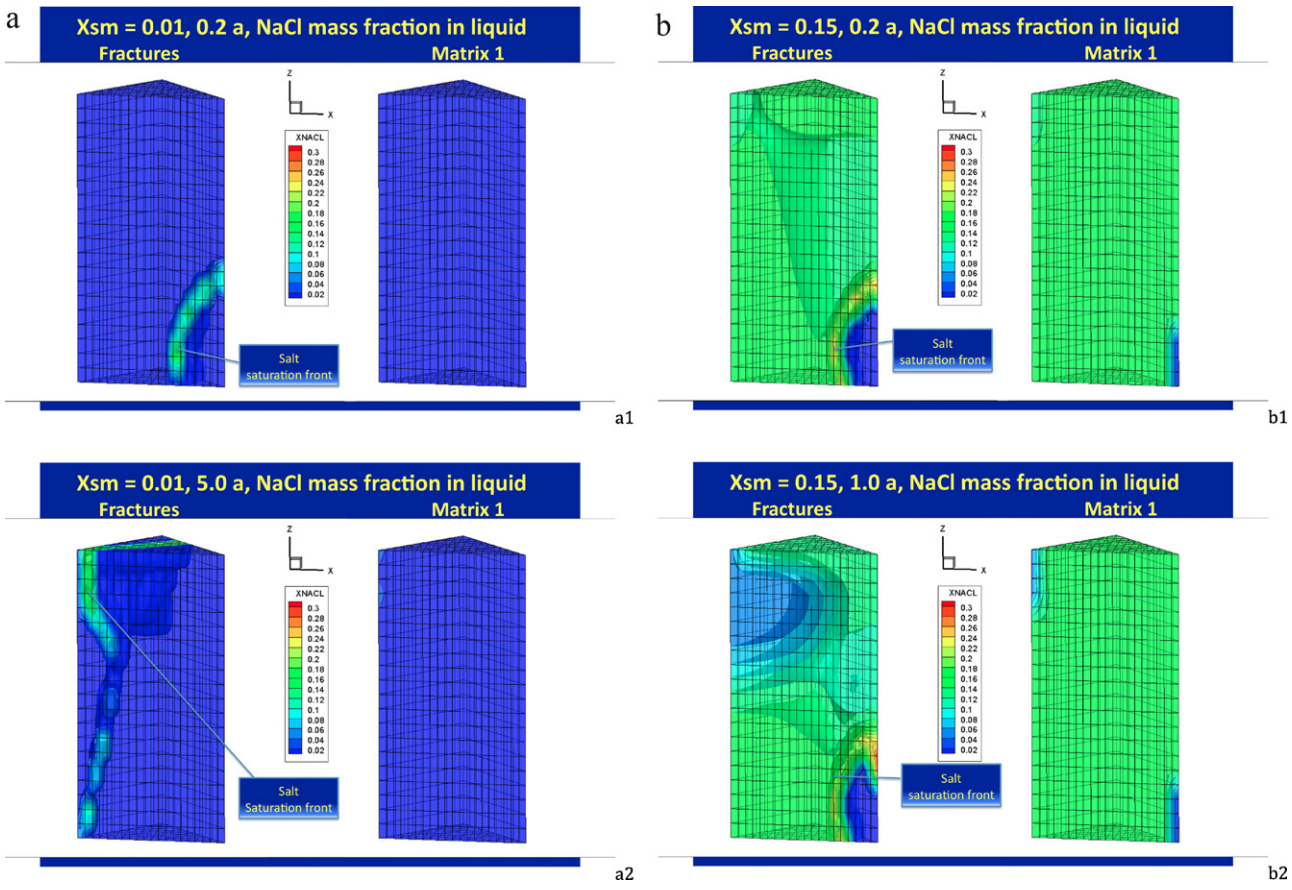

Fig. 6. (a) NaCl mass fraction in the liquid phase within the fracture and 1st matrix continua after 0.2 and 5 years, for a salt mass fraction of 0.01 (see Table 5 for variable definitions). The high-NaCl concentration zone is displaced outward and upward from the injection towards the production well. There is very little salinity increase in the matrix. (b) NaCl mass fraction in the liquid phase within the fracture and 1st matrix continua after 0.2 and 1 year for a salt mass fraction of 0.15 (see Table 5 for variable definitions). The high-NaCl concentration zone remains trapped close to the injection well. Much precipitation occurs everywhere in the model. After 1 year close to the production well the water condenses back to liquid (aqueous phase) diluting the salt concentration of the brine. This effect is the result of the system becoming clogged up. There is no salinity increase in the matrix.

precipitates in the matrix. Within the geochemical limits of the model, we explain this result by observing that there is two-phase flow in the matrix but only single-phase supercritical CO_2 flow in the fractures (see Fig. 5a). Since the permeability of the matrix is much smaller than that of the fractures, the CO_2 flow rate through the matrix is proportionally smaller. Therefore, while the CO_2 phase becomes almost immediately H_2O saturated in the matrix inhibiting any increment in salt concentration, in the fractures, the CO_2 plume remains unsaturated allowing water evaporation. Hence, as the high capillary pressure forces the brine from the matrix into the fractures, water evaporates with consequent increase in NaCl concentration and precipitation at the matrix–fracture interface. The combined effects of the salty-front migration in the fractured reservoir (Fig. 6a) and salt precipitation in the fractures induce salt clogging around the production well after less than 10 years (Figs. 3a and 7a).

(b) At high salinity (Fig. 7b) the precipitation effect is so dominant relative to the salty-front migration that the system becomes clogged up relatively close to the injection well in less than 1 year.

7. Discussion and conclusions

The exploitation of enhanced geothermal systems (EGS) using CO_2 as a working fluid has many potential benefits related to the high compressibility and low viscosity and reactivity of CO_2 at the supercritical conditions of interest (Brown, 2000; Fouillac et al., 2004). Our simulations of such a system confirm that these characteristics more than compensate for the lower heat capacity of CO_2 relative to H_2O, and allow a significant enhancement in the heat extraction rate relative to that obtained by a facility which is run using a formation brine (Apps and Pruess, 2011; Spycher and Pruess, 2011; Wan et al., 2011; and references therein). In addition, there are compounding benefits for the environment from generating more energy from geothermal systems to offset CO_2 emissions from fossil-fuel combustion, while at the same time utilizing captured anthropogenic CO_2.

However, our numerical simulations suggest that salt precipitation can play an unfavorable role if CO_2 is used for heat extraction from EGS in fractured crystalline rocks. While the brine is easily displaced from the fractures by the CO_2 plume, the brine tends to be drawn out from the matrix by capillary forces. Therefore, because of the resulting very low flow rate in the matrix, the CO_2 supercritical phase remains water saturated in the matrix, inhibiting H_2O evaporation into the CO_2-rich phase, further brine concentration, and halite precipitation in the matrix. Instead, as soon as the brine reaches the fractures, it evaporates into the dry, high-flow-rate CO_2 stream, precipitating halite, which tends to clog up the fractures and inhibit fluid flow.

Similar phenomena have been described by Kleinitz et al. (2001) for gas producing wells, by Lorentz and Muller (2003) around injection wells in natural gas storage aquifers, by Xu et al. (2004) around geothermal injection wells, and by Carpita et al. (2006) and

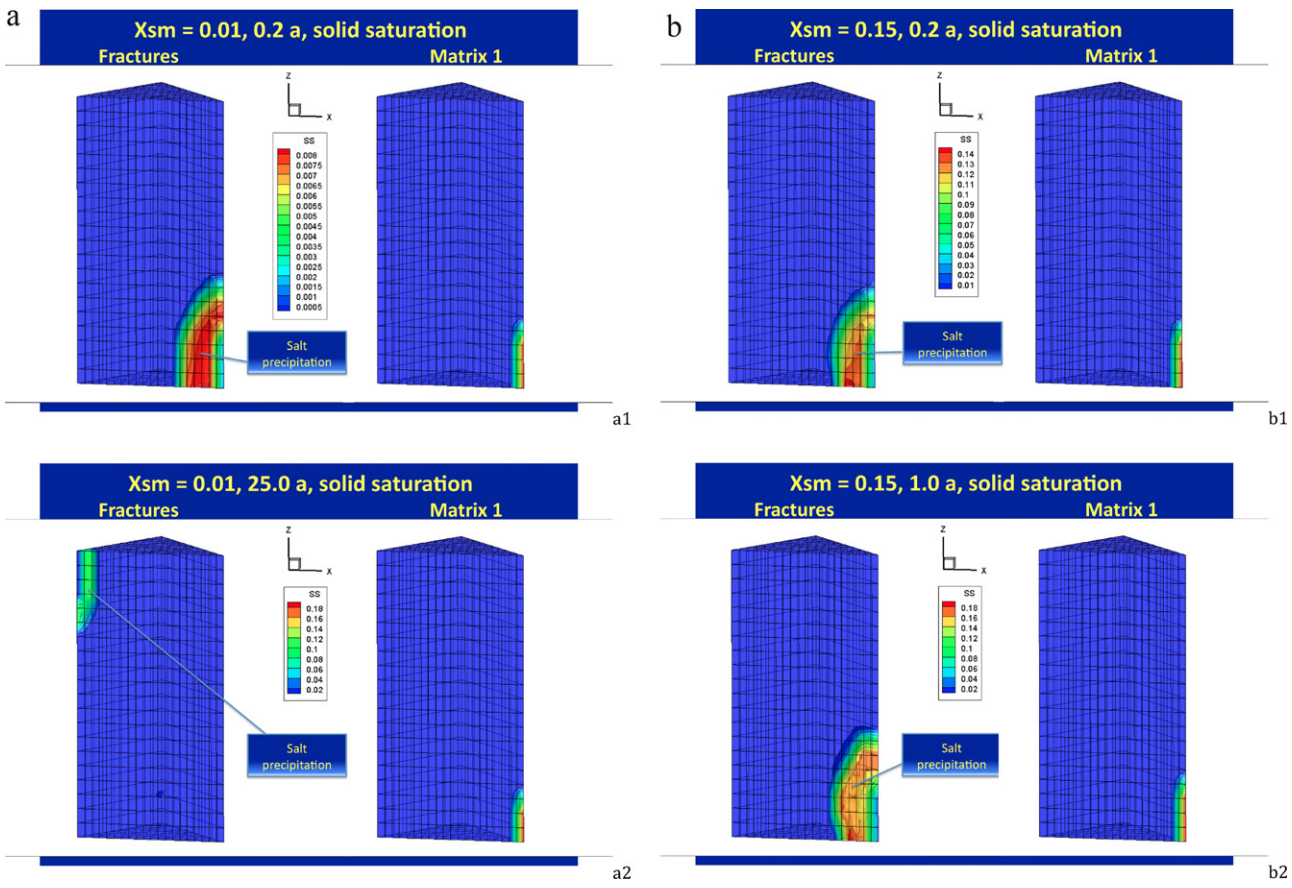

Fig. 7. (a) Halite solid saturation within the fracture and 1st matrix continua after 0.2 and 25 years, for a salt mass fraction of 0.01 (see Table 5 for variable definitions). After 25 years the halite plugs the fractures close to the production well. There is very little salt precipitation in the rest of the volume. (b) Halite solid saturation within the fracture and 1st matrix continua after 0.2 and 1 year for a salt mass fraction of 0.15 (see Table 5 for variable definitions). After only 1 year the halite plugs the fractures close to the injection well. There is very little salt precipitation in the rest of the volume.

Giorgis et al. (2007) for geologic carbon sequestration in depleted-gas reservoirs. In general, however, these studies were limited to two-dimensions, isothermal conditions, or did not include matrix and fracture flow. Therefore, they produced results that are apparently different. The later two studies, in particular, found that only when the brine has high mobility, can it recharge the halite precipitation front as it flows towards the injection well. Our study shows that at low salinities, the saturation/precipitation front is displaced toward the production well, where as time passes it clogs up the rock fractures. At high salinities, water displacement from the matrix and subsequent halite precipitation in the fractures overwhelms the effect of precipitation-front displacement, inducing fracture clogging in proximity of the injection well. In our simulations, salt precipitation plays a much larger role compared to what was previously suggested by Brown (2000).

For systems with low salinity, the gain in efficiency achieved by using CO_2 as the working fluid in EGS in place of the reservoir brines is not significantly affected by clogging. At the time of maximum heat production this gain is over 360%, while for the lifetime of the well (about 6 years) the gain is about 270%. However, the gain in efficiency is drastically reduced at higher salinities, becoming practically insignificant at the highest salt mass fractions modeled in our experiments. In fact, even though the gain at maximum heat production is still 25%, the total heat produced over the short lifetime of the well (less than 1 year) is 15% less than the heat produced with formation brine over this time period. However, since in the recycled brine case the lifetime of well is much longer, significantly more total heat is produced. In both low and high salinity cases, devising reservoir development strategies for inhibiting precipitation and enhancing dissolution in fractures appear to be fundamental requirements for CO_2-EGS.

Our results for the low salinity case show that CO_2-EGS is about 3 times more efficient than H_2O-EGS, a value that apparently falls at the lower end of what had been previously suggested by Randolph and Saar (2011), in a set of numerical simulations which substantially differ from the present ones. This is probably a consequence of starting our simulations with a brine-saturated (as opposed to a CO_2-saturated) reservoir, and including salt precipitation during CO_2 reservoir development within matrix and fractures. In addition, our model runs are at a higher temperature and include buoyancy effects using a larger pressure gradient between injection and production wells relative to former studies (4 MPa instead of 2 MPa in addition to the hydrostatic pressure difference). Note that the function we have chosen to describe the porosity and permeability reduction, the bundle of tubes model (Verma and Pruess, 1988), represents a worst-case scenario because it allows complete clogging of the throats between pores at only 20% solid saturation.

Our results are different in some respects from those obtained by Wan et al. (2011). Their study is not 3D but it includes reactive-transport. The persistence of two-phase conditions in the matrix for relatively longer times facilitates rock-fluid reactions which are not taken into account in our model; on the other hand, buoyancy effects in the CO_2 plume may result in rapid and distinct flow patterns that were not considered by Wan et al. (2011). Combining these two effects, in addition to analyzing the influence on reservoir clogging for different porosity/permeability functions, will be the focus of future work.

Our numerical simulation show that in both low- and high-salinity cases, clogging occurs in very specific areas of the reservoir, namely close to the production and to the injection wells for low and high salinity, respectively. Assuming that salt precipitation and clogging effects are a real consequence of using CO_2 in EGS, the knowledge of the location of the potentially clogged-up volume within the reservoir will facilitate the application of remediation measures directed at avoiding precipitation, dissolving the plugs, and/or mechanically reopening the fractures. Indeed, although our simulations did not include any geomechanical effects, it is possible that fracture creation and reactivation that accompany CO_2-EGS operations might contribute to maintain the fractures open, despite NaCl precipitation that tends to plug them. Future work will focus on devising reservoir management strategies for avoiding or dissolving salt plugs.

Acknowledgments

We are grateful to Patrick Dobson (LBNL) for providing insightful internal review and comments on an earlier draft, and to two anonymous reviewers whose comments allowed us to clarify the presentation. This work was supported by the American Recovery and Reinvestment Act (ARRA), through the Assistant Secretary for Energy Efficiency and Renewable Energy (EERE), Office of Technology Development, Geothermal Technologies Program, of the U.S. Department of Energy under Contract No. DE-AC02-05CH11231.

Appendix A.

To simulate flow in fractures and in matrix pores, we use a dual-porosity (Warren and Root, 1963) multiple interacting continua approach (MINC; Pruess and Narasimhan, 1982, 1985) with parameters and Voronoi grid generated by Wingridder software (Pan, 2007). Accordingly, in this simple model, each grid block is further subdivided into a "string" of five nested sub-blocks. The first of these represents the fracture continuum, which is connected to the neighboring fracture grid sub-blocks. The following four ($N_m = 4$) grid sub-blocks represent the matrix continua, which are connected in series to each other and to the fracture continuum (Fig. 6). Therefore, at the scale of the model, flow occurs along fractures, while at the scale of the grid block, flow occurs between the various matrix sub-blocks and from the first matrix sub-block to the fracture grid sub-block. Fracture spacing is assumed to be 10 m in each of the three coordinate directions. This spacing is perhaps a lower limit for fracture spacing in EGS (Sanyal and Butler, 2005). It is chosen to minimize salt precipitation due to CO_2 reservoir development. For larger fracture spacing, salt precipitation becomes even more relevant. Wingridder calculates the volumes of each of the N_m grid sub-blocks by defining a partition factor (λ_j) as:

$$\lambda_j = \frac{\alpha^{j-1}}{\sum_{i=1}^{i=N_m} \alpha^{i-1}}, \quad \text{with} \quad j = 1 \quad \text{to} \quad N_m, \tag{A1}$$

where j is the grid block number and α is the split factor, which we choose equal to 2, so each grid sub-block has a volume twice that of the preceding one. The volume of each grid sub-block becomes then

$$V_j = \lambda_j \times V_m \tag{A2}$$

where V_m is the total volume of the matrix. To obtain the distance (x_j) from the fracture to the jth matrix sub-block it is sufficient to invert the proximity function $prox(x_j)$ given as:

$$prox(x_j) = \sum_{i=1}^{i=j} \lambda_i \tag{A3}$$

The interface area between subsequent grid sub-blocks is given by

$$A_{j,j+1} = V_m \left. \frac{d[prox(x)]}{dx} \right|_{x_j}, \quad j = 1, (N_m - 1) \tag{A4}$$

Finally, the semi-thickness of each matrix shell (d_j), that is the distance between the sub-block node and the interfaces with the neighboring sub-blocks, is defined as

$$d_j = \frac{x_j - x_{j-1}}{2}, \quad j = 1, (N_m - 1) \quad \text{and} \quad x_0 = 0. \tag{A5}$$

The distance between the fracture node and the 1st matrix sub-block is set equal to zero. The nodal distance of the innermost grid sub-block is calculated based on the quasi-steady state flow theory as

$$d_m = \frac{3U_1U_2U_3}{U_1U_2 + U_2U_3 + U_1U_3}, \quad \text{where} \quad U_i = a_i - 2x_{Nm} \quad \text{and} \quad i = 1, 2, 3. \tag{A6}$$

References

Apps, J., Pruess, K., 2011. Modeling geochemical processes in enhanced geothermal systems with CO_2 as heat transfer fluid. In: Proceedings of the Thirty-sixth Workshop on Geothermal Reservoir Engineering, Stanford University, Stanford, CA, January 31–February 2, SGP-TR-191.

Atrens, A.D., Gurgenci, H., Rudolph, V., 2008. Carbon dioxide thermosiphon optimization. In: Australian Geothermal Energy Conference, pp. 149–152.

Atrens, A.D., Gurgenci, H., Rudolph, V., 2009. CO_2 thermosiphon for competitive geothermal power generation. Energy & Fuels 23, 553–557.

Atrens, A.D., Gurgenci, H., Rudolph, V., 2010. Electricity generation using a carbon-dioxide thermosiphon. Geothermics 39, 161–169.

Brown, D., 2000. A hot dry rock geothermal energy concept utilizing supercritical CO_2 instead of water. In: Proceedings of the Twenty-fifth Workshop on Geothermal Reservoir Engineering, Stanford University, CA, USA, pp. 233–238.

Carpita, M., Giorgis, T., Battistelli, A., 2006. Modeling CO_2 injection with halite precipitation using an extended Verma & Pruess porosity–permeability model. In: Proceedings of the TOUGH2 Symposium, Lawrence Berkeley National Laboratory, Berkeley, CA, USA, May 15–17.

Corey, A.T., 1954. The interaction between gas and oil relative permeabilities. Producers Monthly November, 38–41.

Fouillac, C., Sanjuan, B., Gentier, S., Czernichowski-Lauriol, I., 2004. Could sequestration of CO_2 be combined with the development of enhanced geothermal systems? In: Paper presented at the Third Annual Conference on Carbon Capture and Sequestration, Alexandria, VA, USA, May 3–6.

Giorgis, T., Carpita, M., Battistelli, A., 2007. 2D modeling of salt precipitation during the injection of dry CO_2 in a depleted gas reservoir. Energy Conversion and Management 48, 1816–1826.

Kleinitz, W., Köheler, M., Dietzsch, G., 2001. The precipitation of salt in gas producing wells. In: Paper presented at the SPE European Formation Damage Conference, La Hague, Netherlands, May 21–22, SPE 68953.

Lorentz, S., Muller, W., 2003. Modeling of halite formation in natural gas storage aquifers. In: Proceedings of the TOUGH2 Symposium, Lawrence Berkeley National Laboratory, Berkeley, CA, USA, May 12–14.

Magliocco, M., Kneafsey, T., Pruess, K., Glaser, S., 2011. Laboratory experimental study of heat extraction from porous media by means of CO_2. In: Proceedings of the Thirty-sixth Workshop on Geothermal Reservoir Engineering, Stanford University, Stanford, CA, January 31–February 2, SGP-TR-191.

Pan, L., 2007. User information document for: Wingridder version 3.0. Doc. ID 10024-UID-3.0-0, 76 pp.

Pritchett, J.W., 2009. On the relative effectiveness of H_2O and CO_2 as reservoir working fluids for EGS heat mining. Geothermal Resources Council Transactions 33, 235–239.

Pruess, K., 2006. Enhanced geothermal systems (EGS) using CO_2 as working fluids – a novel approach for generating renewable energy with simultaneous sequestration of carbon. Geothermics 35, 351–367.

Pruess, K., Narasimhan, T.N., 1982. On fluid reserves and the production of superheated steam from fractured vapor-dominated geothermal reservoirs. Journal of Geophysical Research 87 (B11), 9329–9339.

Pruess, K., Narasimhan, T.N., 1985. A practical method for modeling fluid and heat flow in fractured porous media. Society of Petroleum Engineering Journal 25 (6), 14–26.

Pruess, K., Azaroual, M., 2006. On the feasibility of using supercritical CO_2 as heat transmission fluid in an engineered hot dry rock geothermal system. In: Proceedings of the Thirty-first Workshop on Geothermal Reservoir Engineering, Stanford University, Stanford, CA, USA, January 30–February 1, pp. 386–393.

Pruess, K., Spycher, N., 2007. ECO_2N – a fluid property module for the TOUGH2 code for studies of CO_2 storage in saline aquifers. Energy Conversion and Management 48, 1761–1767.

Pruess, K., Spycher, N., 2010. Enhanced geothermal systems (EGS) with CO_2 as a heat transmission fluid – a scheme for combining recovery of renewable energy with geologic storage of CO_2. In: Proceedings World Geothermal Congress, Bali, Indonesia, April 25–29.

Pruess, K., Oldenburg, C., Moridis, G., 1999. TOUGH2 User's Guide – Version 2.0. LBNL-43134, 198 pp.

Randolph, J.B., Saar, M.O., 2011. Combining geothermal energy capture with geologic carbon dioxide sequestration. Geophysical Research Letters 38, http://dx.doi.org/10.1029/2011GL047265, L10401.

Rosenbauer, R.J., Koksalan, T., Palandri, J.L., 2005. Experimental investigation of CO_2–brine–rock interactions at elevated temperature and pressure: implications for CO_2 sequestration in deep-saline aquifers. Fuel Processing Technology 86, 1581–1597.

Safe Drinking Water Act (SDWA), 1974. P.L. 93-523, 88 Stat. 1660. <http://www.answers.com/topic/safe-drinking-water-act#ixzz1ge6mFyc0> (accessed 6.5.12).

Sanyal, S.K., Butler, S.J., 2005. An analysis of power generation prospects from enhanced geothermal systems. In: Proceedings of World Geothermal Congress, Antalya, Turkey, April 24–29, pp. 1–6.

Spycher, N., Pruess, K., 2011. A model for thermophysical properties of CO_2–brine mixtures at elevated temperatures and pressures. In: Proceedings of the Thirty-sixth Workshop on Geothermal Reservoir Engineering, Stanford University, Stanford, CA, January 31–February 2, SGP-TR-191.

van Genuchten, M.Th., 1980. A closed-form equation for predicting the hydraulic conductivity of unsaturated soils. Soil Sciences Society 44, 892–898.

Verma, A., Pruess, K., 1988. Thermohydrologic conditions and silica redistribution near high-level nuclear wastes emplaced in saturated geological formations. Journal of Geophysical Research 93 (B2), 1159–1173.

Wan, Y., Xu, T., Pruess, K.,2011. Impact of fluid-rock interactions on enhanced geothermal systems with CO_2 as heat transmission fluid. In: Proceedings of the Thirty-sixth Workshop on Geothermal Reservoir Engineering. Stanford University, Stanford, CA, January 31–February 2, SGP-TR-191.

Warren, J.E., Root, P.J., 1963. The behavior of naturally fractured reservoir. Society of Petroleum Engineering Journal Transactions, AIME 228, 245–255.

Xu, T., Ontoy, Y., Molling, P., Spycher, N., Parini, M., Pruess, K., 2004. Reactive transport modeling of injection well scaling and acidizing at Tiwi field, Philippines. Geothermics 33, 477–491.

Xu, T., Pruess, K., Apps, J., 2008. Numerical studies of fluid–rock interactions in enhanced geothermal systems (EGS) with CO_2 as working fluid. In: Proceedings of the Thirty-third Workshop on Geothermal Reservoir Engineering, Stanford University, Stanford, CA, January 28–30, SGP-TR-185.

Xu, T., Pruess, K., 2010. Reactive transport modeling to study fluid–rock interactions in enhanced geothermal systems (EGS) with CO_2 as working fluid. In: Proceedings of World Geothermal Congress 2010, Bali, Indonesia, April 25–29.

Xu, T., Zhang, W., Pruess, K., 2010. Numerical simulation to study feasibility of using CO_2 as stimulation agent for enhanced geothermal systems. In: Proceedings of the Thirty-fifth Workshop on Geothermal Reservoir Engineering, Stanford University, Stanford, CA, February 1–3, SGP-TR-188.